INTERNATIONAL JOURNAL FOR NUMERICAL METHODS IN FLUIDS, VOL. 27, 193–206 (1998)

COMPUTATION OF UNSTEADY FLOWS WITH MIXED FINITE VOLUME/FINITE ELEMENT UPWIND METHODS

CHRISTOPHE DEBIEZ*, ALAIN DERVIEUX, KATHERINE MER AND BONIFACE NKONGA

INRIA Sophia-Antipolis, BP 93, F-06902 Valbonne Cedex, France

SUMMARY

We refer to as mixed element/volume (MEV) methods the application of finite element for diffusion terms and finite volume for advection terms in a flow model. The compatibility of these methods can be checked for some low-order approximations; the resulting schemes may enjoy the relative mesh-regularity-independent accuracy of finite element methods as discussed in a first section. In recent years a number of developments (by INRIA Dassault and T. Barth, among others) have produced P1-continuous schemes that involve some MUSCL/TVD unidirectional limitation; the resulting schemes are very useful but sometimes may involve much more numerical viscosity than necessary, especially for unsteady computations. In the present study, a new version is built by using a larger molecule for the intercell flux evaluation. The 1D version can be promoted to fourth- or even fifth-order spatial accuracy. The 2D version is no better than second-order-accurate; however, it involves only a sixth-order dissipation and the global accuracy is markedly improved even on irregular meshes. The above development extends the ability of the MUSCL/MEV scheme towards the accurate calculation of unsteady flows involving vortex shedding. © 1998 John Wiley & Sons, Ltd.

Int. J. Numer. Meth. Fluids, **27**, 193–206 (1998)

KEY WORDS: finite element; finite volume; numerical dissipation; compressible flow

1. INTRODUCTION

The simulation of aerodynamic processes has been concentrated for a long time on steady flows, the unsteady ones often being considered as a less important extension of simulation tool functionalities. This tendency is also found in early finite element studies, for which the basic idea was an equilibrium idea.

The explosive increase in the development of upwind methods, particularly Godunov-type ones, able to solve accurately and stably unsteady Riemann problems (the famous 'shock tube') has undoubtedly changed the focus of scheme design.

Most of the new schemes related to Riemann solvers or artificial viscosity involve a fourth-order difference as dissipative term. This type of stabilization can also be used in finite element (FE) formulations and one first important question is whether the usual properties of the FE approximation are deteriorated by the stabilization term. This will be studied in the next section of this paper.

*Correspondence to: C. Debiez, INRIA Sophia-Antipolis, BP 93, F-06902 Valbonne Cedex, France.

CCC 0271–2091/98/010193–14 $17.50 *Received May 1996*

The above fourth-order difference dissipation carries a third-order truncation error that can be dominant in the computations, even in second-order-accurate 2D approximations; a lot of works recently have aimed at reducing the impact of this kind of dissipation. In the case of steady calculations in which the advected quantities are relatively constant along characteristics, marked improvements can be obtained by reducing cross-wind dissipation.[1,2] For truly unsteady flows we think it's interesting to investigate higher-order stabilization. Section 3 is devoted to the study of high-order upwinding to be combined with a finite element/finite volume formulation.

To demonstrate the ability of these new developments, a set of steady and unsteady flows is presented in Section 4.

2. STABILIZATION BY HIGHER-ORDER DISSIPATION

We consider a finite element scheme stabilized by a fourth-difference dissipation term. The problems of interest are the convection–diffusion and convection-dominated stationary problems. The analysis can, however, be extended without additional difficulty to the unsteady case. Some of the results presented are developed in Reference 3. These results show that there exists a choice of fourth-order dissipations that preserve the accuracy properties of the Galerkin method.

2.1. Stabilized Galerkin method

We consider the convection–diffusion boundary value problem

$$-\varepsilon\Delta u + \operatorname{div}(\vec{V}u) = f \quad \text{in } \Omega, \qquad u = 0 \quad \text{on } \Gamma. \tag{1}$$

For the reduced problem ($\varepsilon = 0$) the boundary conditions are defined on the inflow boundary. We consider a discrete linear continuous operator $\Delta^h\colon\ C^0(\bar{\Omega}) \to L^2(\Omega)$ associated with the triangulation $\mathscr{T}^h$ and we introduce a symmetrical bilinear form b_h defined on $V^h \times V^h$ by

$$b_h(u_h, v_h) = h^\alpha \iint_\Omega \Delta^h u_h \Delta^h v_h \, \mathrm{d}\vec{x},$$

where α is a real positive constant and V^h is the usual P1 finite element space function. The numerical scheme under study is inspired by the variational finite difference method of Céa and is written as follows:

$$\begin{gathered} \text{find } u_h \in V_0^h \text{ such that} \\ a_h(u_h, v_h) = l(v_h) \quad \text{for all } v_h \in V_0^h, \end{gathered} \tag{2}$$

where

$$a_h(u_h, v_h) = a(u_h, v_h) + b_h(u_h, v_h). \tag{3}$$

Here a is the bilinear form associated with the weak form of (1). Assumptions on the velocity vector field $\vec{V}$ insure the existence and uniqueness of a solution $u_h \in V_0^h$ of problem (2), (3).

2.2. Convection–diffusion case

We shall present here global error estimates in the $H^1(\Omega)$-norm and $L^2(\Omega)$-norm under the following assumptions on the finite difference operator Δ^h:

$$|\Delta^h v_h|_{0,\Omega} \leqslant C_1 h^{-1} \|v_h\|_{1,\Omega} \quad \text{for all } v_h \in V_0^h, \tag{4a}$$

$$|\Delta^h \varphi|_{0,\Omega} \leqslant C_2 h^{-m} \|\varphi\|_{2,\Omega} \quad \text{for all } \varphi \in H^2(\Omega), \tag{4b}$$

where C_1 and C_2 are independent of h and m is a non-negative integer. The first estimate is a discrete inverse estimate without any quasi-uniform assumption on the triangulation. For a divided second-order finite difference operator, inequality (4b) is obvious with $m=2$, but depending on the 'quality' of the discrete operator Δ^h, it may be obtained with $m=1$ or $m=0$, the case $m=0$ being an optimal case (see below). In the theorems below the triangulation is assumed to be regular in the usual sense and assumptions for coercivity of a are considered on the velocity vector field $\vec{V}$.

Theorem 1

Suppose the assumptions (4) are verified. Let u be the exact solution of (1) and u_h be the solution of the approximate problem (2), (3). Suppose that the polygonal domain Ω has convex corners and $n \leqslant 3$. If $\alpha \geqslant 2+m$, then

$$\|u - u_h\|_{1,\Omega} \leqslant Ch\|u\|_{2,\Omega}.$$

Furthermore, if $\alpha \geqslant 2+2m$, then

$$|u - u_h|_{0,\Omega} \leqslant Ch^2\|u\|_{2,\Omega}.$$

2.3 Convection-dominated case

Theorem 2

Suppose the assumptions (4) are verified. Let u be the exact solution of (1) with $0 \leqslant \varepsilon \leqslant 1$. Let u_h be the solution of the approximate problem (2), (3). Suppose that the polygonal domain Ω has convex corners and $n \leqslant 3$. If $\alpha \geqslant 2+2m$, then

$$|u - u_h|_{0,\Omega} \leqslant Ch\|u\|_{2,\Omega} \quad C \text{ independent of } \varepsilon.$$

Furthermore, if $\alpha \geqslant 3+2m$ and $h \leqslant h_0(\varepsilon)$, then

$$|u - u_h|_{0,\Omega} \leqslant C\frac{h^2}{\sqrt{\varepsilon}}\|u\|_{2,\Omega}, \quad C \text{ independent of } \varepsilon.$$

The condition $h \leqslant h_0(\varepsilon)$ is in fact the usual condition on the cell Peclet number.

2.4. Jameson-type dissipation operator

The fourth-difference Jameson-type dissipation for unstructured meshes is written as the square of a second-order dissipation operator:[4]

$$D^4(u_i) = h^3 m(C_i)\Delta_i^h[\Delta^h u_h],$$

where

$$\Delta_k^h u = \sum_{k\in V_i} \sum_{j\in V_k} \frac{u_j - u_k}{\text{meas}(C_k)}$$

and C_i is a cell around point P_i, an element of a dual triangulation of $\mathcal{T}_h$. The dissipative term can also be written in the expanded form

$$D^4(u_i) = h^3 \sum_{k\in V_i} \sum_{j\in V_k} \frac{u_j - u_k}{\text{meas}(C_k)} - h^3 \text{ card}(V_i) \sum_{k\in V_i} \frac{u_k - u_i}{\text{meas}(C_i)}. \tag{5}$$

Given a triangulation $\mathcal{T}_h$, let us define the finite difference second-order operator Δ^h in the following manner: for all continuous functions v, $\Delta^h v$ is a step function, constant over each cell C_i and defined by

$$\Delta^h v \equiv \sum_{j\in V_i} \frac{v(x_j) - v(x_k)}{\text{meas}(C_i)} \quad \text{on } C_i, \tag{6}$$

which gives the perturbation FE term $b_h(u_h, \phi_{ih}) = h^\alpha m(C_i)\Delta_i^h[\Delta^h u_h]$. We recognize the Jameson-type dissipation if $\alpha = 3$. For the discrete operator Δ^h: $C^0(\Omega) \to L^2(\Omega)$ given by (6), properties (4) are verified with $m = 1$ in the general case and with $m = 0$ for uniform Cartesian triangulations such that each node has a symmetrical set of neighbours and if no dissipation is introduced for the boundary points.

The optimal accuracy obtained with $m = 0$ in property (4b) can be connected with the so-called linearity preservation (LP) property that designs second-order-accurate convection schemes for steady solutions.[5] In Reference 6, we prove that the property LP implies local consistency for convection equations; furthermore, the order of consistency can be arbitrarily large for a scheme that preserves polynomials of arbitrarily large order. We conjecture that the methodology presented in this paper could be extended to the study of higher-order dissipation terms that can be written in a symmetrical variational form, provided that more regularity assumptions on the solution are made.

Coefficients for the dissipation in a variational form can be obtained that insure good accuracy for stretched meshes in boundary layers.[7] These coefficients of the fourth-order dissipation can be compared with those obtained for MUSCL-type or Jameson-type schemes on Friedrichs–Keller Cartesian meshes and provide a theoretical justification of the behaviour of these schemes on stretched meshes.[7]

3. STILL-HIGHER-ORDER DISSIPATION

The main motivation of this study is the following. In many computations relying on second-order Godunov, the numerical error is carried by the dissipation. We can get inspired by direct simulation techniques in which filters correspond to very-high-even-order derivatives. In this paper we consider upwind schemes of MUSCL type that involve sixth-order dissipations.

3.1. 2D unstructured case

The numerical integration with an upwind scheme generally leads to approximations which are only first-order-accurate. Van Leer has proposed some extensions of these schemes in order to get a second-order-accurate solution. According to the MUSCL technique, one way to reach second-order

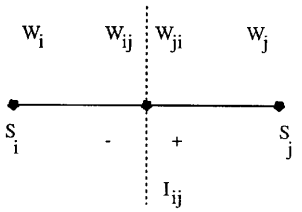

Figure 1. Position of W_{ij} and W_{ji} on $[S_i, S_j]$

accuracy is to evaluate fluxes with extrapolated values W_{ij} and W_{ji} at the interface of the cells (Figure 1):

$$W_{ij} = W_i + \tfrac{1}{2}(\vec{\nabla}W)_{ij} \cdot \vec{ij}, \qquad W_{ji} = W_j - \tfrac{1}{2}(\vec{\nabla}W)_{ji} \cdot \vec{ij}, \tag{7}$$

where the approximate 'slopes' $(\vec{\nabla}W)_{ij,\,ji}$ are obtained using a combination of centred and upwind gradients. In order to increase the accuracy of the basic MUSCL construction, we propose to define these slopes as follows.

The centred gradient $(\vec{\nabla}W)_{ij}^{C}$ is defined as $(\vec{\nabla}W)_{ij}^{C} \cdot \vec{ij} = W_j - W_i$. The nodal gradient $(\vec{\nabla}W)_i$ is calculated on cell C_i as the average of the gradients on the triangles which include the considered node:

$$(\vec{\nabla}W)_i = \frac{1}{\text{area}(C_i)} \sum_{T \in C_i} \frac{\text{area}(T)}{3} \sum_{k \in T} W_k \vec{\nabla}\Phi_k|_T. \tag{8}$$

The upwind gradient is computed according to the definition of the downstream and upstream triangles associated with edge $[S_iS_j]$ (Figure 2). The downstream and upstream triangles are respectively noted T_{ij} and T_{ji}. One has therefore $(\vec{\nabla}W)_{ij}^{D} = \vec{\nabla}W|_{T_{ij}}$ and $(\vec{\nabla}W)_{ij}^{U} = \vec{\nabla}W|_{T_{ij}}$, where

$$\nabla W|_T = \sum_{k \in T} W_k \vec{\nabla}\Phi_k|_T$$

are the P1 Galerkin gradients on triangle T. This option allows extensions to local-extremum-diminishing (LED) schemes as shown in Reference 8.

We now present several new choices for estimating the nodal gradients $(\vec{\nabla}W)_{ij}$ and $(\vec{\nabla}W)_{ji}$.

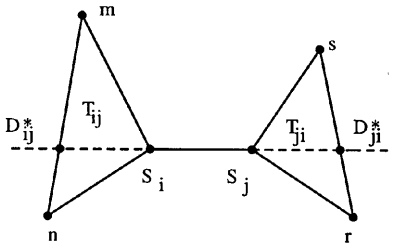

Figure 2. Localization of extra interpolation points D_{ij}^{*} and D_{ji}^{*} of nodal gradients

Method 1 (mixed nodes/triangles)

We propose to enlarge the stencil of the interpolation for taking into account a supplementary upwind gradient. This upwind gradient $(\vec{\nabla}W)_{ij}^{\mathrm{D}^*}$ is computed using the *nodal P1 Galerkin gradients* at the vertices of the edge of triangle T_{ij} which is opposite to vertex S_i (Figure 2):

$$(\vec{\nabla}W)_{ij}^{\mathrm{D}^*} = \frac{\|\overrightarrow{D^*m}\|}{\|\overrightarrow{mn}\|}(\vec{\nabla}W)_m + \frac{\|\overrightarrow{D^*n}\|}{\|\overrightarrow{mn}\|}(\vec{\nabla}W)_n. \tag{9}$$

We then define the gradient $(\vec{\nabla}W)_{ij}$ as (Figure 3)

$$\begin{aligned}(\vec{\nabla}W)_{ij}\cdot\vec{ij} = {} & (1-\beta)(\vec{\nabla}W)_{ij}^{\mathrm{C}}\cdot\vec{ij} + \beta(\vec{\nabla}W)_{ij}^{\mathrm{D}}\cdot\vec{ij} \\ & + \xi^{\mathrm{c}}[(\vec{\nabla}W)_{ij}^{\mathrm{D}}\cdot\vec{ij} - 2(\vec{\nabla}W)_{ij}^{\mathrm{C}}\cdot\vec{ij} + (\vec{\nabla}W)_{ij}^{\mathrm{U}}\cdot\vec{ij}] \\ & + \xi^{\mathrm{d}}[(\vec{\nabla}W)_{ij}^{\mathrm{C}}\cdot\vec{ij} - 3(\vec{\nabla}W)_{ij}^{\mathrm{D}}\cdot\vec{ij} + 2(\vec{\nabla}W)_{ij}^{\mathrm{D}^*}\cdot\vec{ij}].\end{aligned} \tag{10}$$

Method 2 (three upstream triangles)

This method is a variant of method 1. The strategy is based on the computation of the gradients $(\vec{\nabla}W)_{ij}*$ via the upwind gradients $(\vec{\nabla}W)_{ij}^m$ and $(\vec{\nabla}W)_{ij}^n$ which are calculated for the downstream and upstream *triangles* associated with edge $[S_iS_j]$ at points m and n (Figure 4). Then we define

$$(\vec{\nabla}W)_{ij}^{\mathrm{D}^*} = \frac{\|\overrightarrow{D^*m}\|}{\|\overrightarrow{mn}\|}(\vec{\nabla}W)_{ij}^m + \frac{\|\overrightarrow{D^*n}\|}{\|\overrightarrow{mn}\|}(\vec{\nabla}W)_{ij}^n, \tag{11}$$

where

$$(\vec{\nabla}W)_{ij}^m = \vec{\nabla}W|_{T_{ij}^m}, \qquad (\vec{\nabla}W)_{ij}^n = \vec{\nabla}W|_{T_{ij}^n}. \tag{12}$$

The advantage of this method is to have a small stencil with aligned points in the case of Friedrichs–Keller regular meshes.

Method 3 (purely nodal)

The correction is built only with *nodal gradients* (Figure 5):

$$\begin{aligned}(\vec{\nabla}W)_{ij}\cdot\vec{ij} = {} & (1-\beta)(\vec{\nabla}W)_{ij}^{\mathrm{C}}\cdot\vec{ij} + \beta(\vec{\nabla}W)_{ij}^{\mathrm{D}}\cdot\vec{ij} \\ & + \xi^{\mathrm{d}}[(\vec{\nabla}W)_{ij}^{\mathrm{D}^*}\cdot\vec{ij} - 2(\vec{\nabla}W)_i\cdot\vec{ij} + (\vec{\nabla}W)_j\cdot\vec{ij}]\end{aligned} \tag{13}$$

with $(\vec{\nabla}W)_{ij}^{\mathrm{D}^*}$ given by (9).

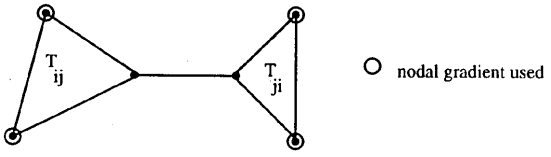

Figure 3. Method 1: downstream triangle, upstream triangle and four nodal gradients

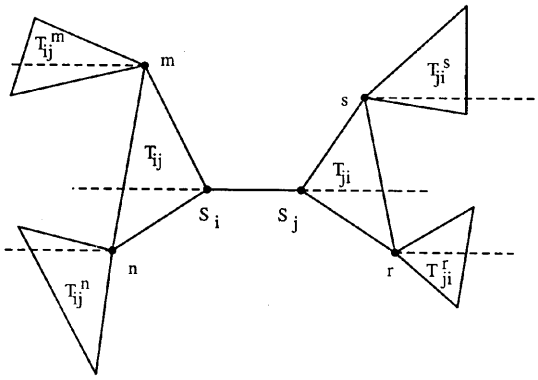

Figure 4. Construction of triangles T_{ij}^m and T_{ij}^n, method 2: three downstream triangles, three upstream triangles

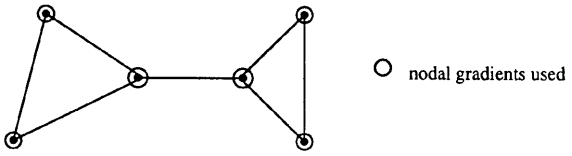

Figure 5. Method 3: six nodal gradients

The coefficients β, ξ^c and ξ^d in (10) and (13) are upwinding parameters that control the combination of fully upwind and centred slopes.

To sum up, these schemes have only sixth-order dissipation and are in general second-order-accurate, but they become higher-order-accurate in the linear case for some values of the parameters β, ξ^c and ξ^d (Table I).[9,10]

Note that in the non-linear case, Wu and Wang have shown that there exists no scheme of MUSCL type with accuracy order higher than two.[11]

Table I. Accuracy of different versions of new scheme in 2D regular case

		β	ξ^c	ξ^d	Order
β-Scheme		1/3	0	0	3
Method 1	Scheme 1	1/3	−1/6	0	4
	Scheme 3	1/3	−1/10	−1/15	3
Method 2	Scheme 1	1/3	−1/6	0	4
	Scheme 2	5/12	0	−1/12	4
	Scheme 3	11/30	−1/10	−1/30	5
Method 3	Scheme 2	1/3	0	−1/6	4
	Scheme 3	1/3	−1/30	−2/15	5

4. NUMERICAL ILLUSTRATION

4.1. Computation of 2D external steady flow

As a steady flow, an inviscid subsonic flow at $M_\infty = 0{\cdot}63$, $\theta = 2{\cdot}0^\circ$ is computed about as NACA 0012 aerofoil using the different versions of the new scheme with a CFL number of about 1000 on various grids. We are interested in the reduction of spurious numerically generated entropy deviation. Three embedded meshes are considered with 800, 3114 and 12,284 nodes, in which finer meshes are obtained by uniform division of the coarser ones (a non-optimal process for mesh quality, just ensuring that the mesh size is divided by two). We present the entropy distributions generated by the schemes on the three meshes (Figures 7, 9 and 11). The flow singularity near the trailing edge is not well captured, but overall improvement is evident. In particular, for the finer mesh, entropy levels turn out to be about two times better with the new schemes. Examination of the Mach contours proves that the new schemes give a better solution with 3114 nodes than does old one with 12,284 (Figures 6, 8 and 10).

4.2. Computation of 2D unsteady flow

We present here the numerical simulation of the impulsive starting of an NACA 0012 aerofoil at high angle of attack and low Mach number. The flow is also unsteady and evolves in a situation where vortices appear. The flow conditions that we consider are given by $M_\infty = 0{\cdot}1$, $\theta = 30^\circ$, $Re = 1000$ and the adimensional time ($V_\infty = 1$ m s^{-1}) is 3 s.

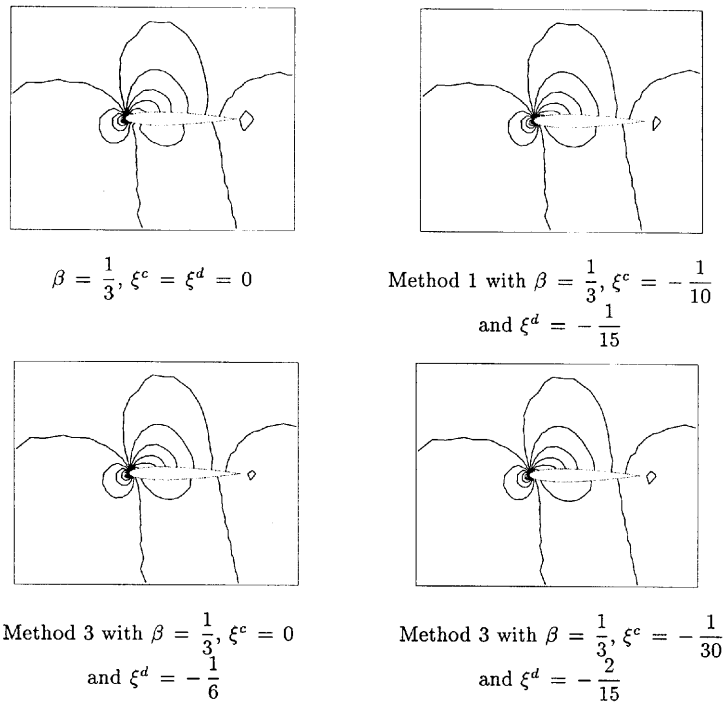

Figure 6. Mach contours about NACA 0012 aerofoil using different versions of new scheme on mesh with 800 nodes: 40 Mach contours, $\Delta M = 0{\cdot}05$, $M_m = 0{\cdot}025$, $M_M = 1{\cdot}975$

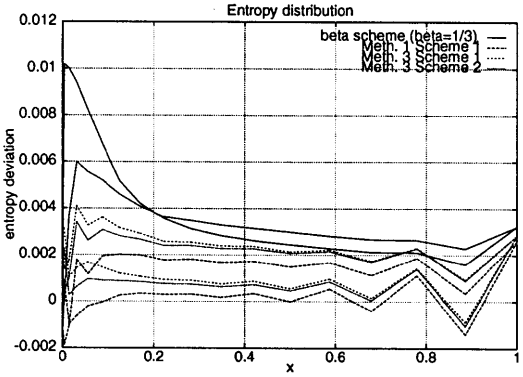

Figure 7. Entropy distribution generated by different schemes: subsonic aerofoil flow at $M_\infty = 0{\cdot}63$, 2° on mesh with 800 nodes

The extra accuracy is first demonstrated on a coarse unstructured mesh with 3114 vertices (Figure 12). With a finer mesh (12,284 vertices), scheme 3 is able to capture most of the details of this complex flow (Figure 13).

4.3. Aeroelastic applications

A fluid–structure interaction problem for a NACA 0012 aerofoil is considered.[12] The fluid is modelled by the Euler equations. We assume that the aerofoil has two degrees of freedom: the vertical translation h of the elastic centre and the rotation α (Figure 14).

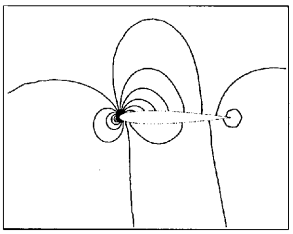

$\beta = \frac{1}{3}, \xi^c = \xi^d = 0$

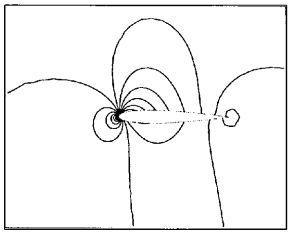

Method 1 with $\beta = \frac{1}{3}, \xi^c = -\frac{1}{10}$ and $\xi^d = -\frac{1}{15}$

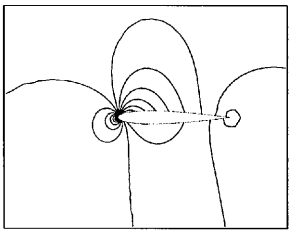

Method 3 with $\beta = \frac{1}{3}, \xi^c = 0$ and $\xi^d = -\frac{1}{6}$

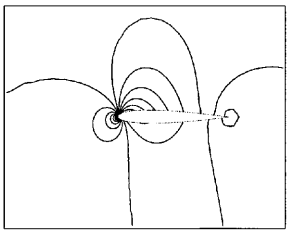

Method 3 with $\beta = \frac{1}{3}, \xi^c = -\frac{1}{30}$ and $\xi^d = -\frac{2}{15}$

Figure 8. Mach contours about NACA 0012 aerofoil using different versions of new scheme on mesh with 3114 nodes: 40 Mach contours, $\Delta M = 0{\cdot}05$, $M_m = 0{\cdot}025$, $M_M = 1{\cdot}975$

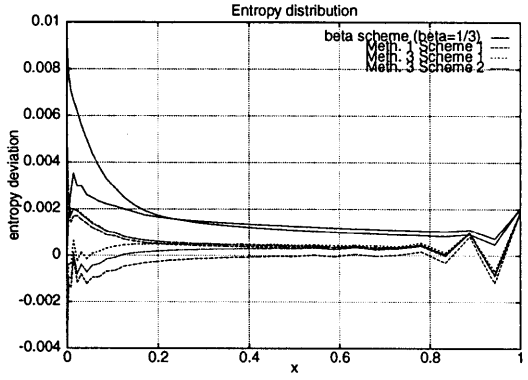

Figure 9. Entropy distribution generated by different schemes: subsonic aerofoil flow at $M_\infty = 0{\cdot}63$, 2° on a mesh with 3114 nodes

The fluid–structure interaction problem is described by the system

$$\begin{aligned} &\frac{\partial}{\partial t} W + \frac{\partial}{\partial x} F(W) + \frac{\partial}{\partial y} G(W) = 0, \\ &M\ddot{q}(t) + C\dot{q}(t) + Kq(t) = Q(W(t)), \end{aligned} \tag{14}$$

where W is the vector of conservative flow variables, q is the displacement vector and Q is the generalized force vector.

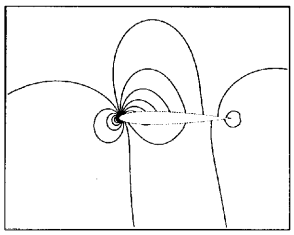

$\beta = \frac{1}{3}, \xi^c = \xi^d = 0$

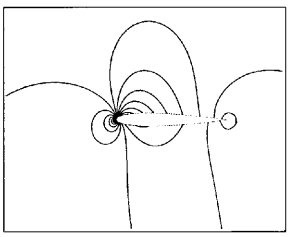

Method 1 with $\beta = \frac{1}{3}, \xi^c = -\frac{1}{10}$ and $\xi^d = -\frac{1}{15}$

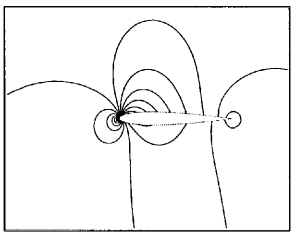

Method 3 with $\beta = \frac{1}{3}, \xi^c = 0$ and $\xi^d = -\frac{1}{6}$

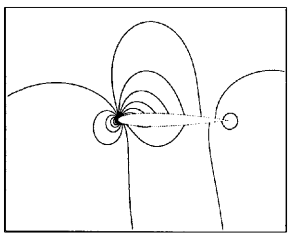

Method 3 with $\beta = \frac{1}{3}, \xi^c = -\frac{1}{30}$ and $\xi^d = -\frac{2}{15}$

Figure 10. Mach contours about NACA 0012 aerofoil using different versions of new scheme on mesh with 12,284 nodes: 40 Mach contours, $\Delta M = 0{\cdot}05$, $M_\mathrm{m} = 0{\cdot}025$, $M_\mathrm{M} = 1{\cdot}975$. The solutions calculated with the new scheme on the mesh with 3114 nodes (Figure 8) are as good as the computation with the old scheme on the mesh with 12,284 nodes

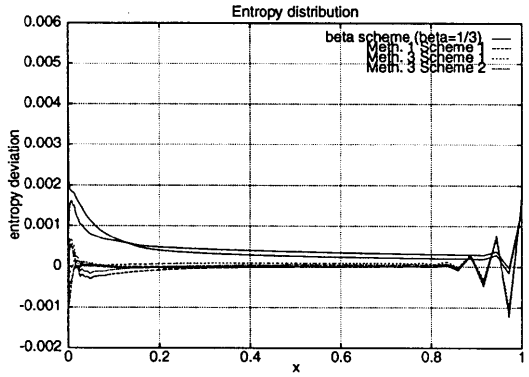

Figure 11. Entropy distribution generated by different schemes: subsonic aerofoil flow at $M_\infty = 0{\cdot}63$, 2° on mesh with 12,284 nodes

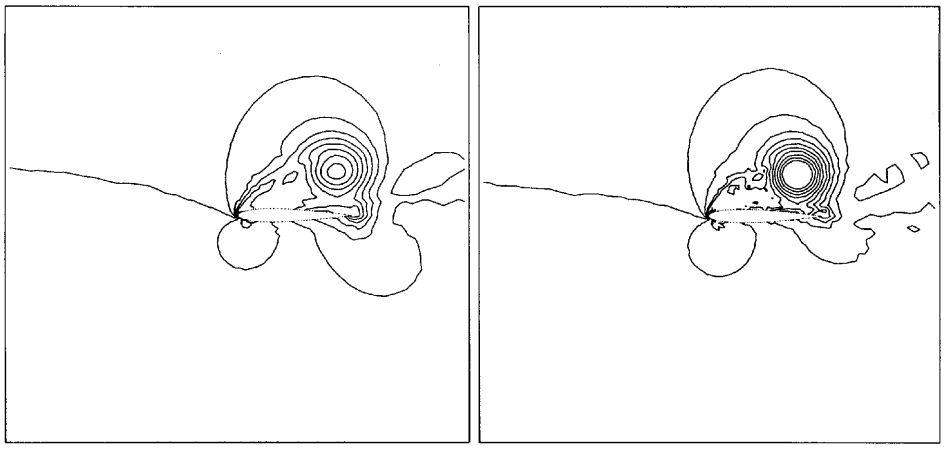

Figure 12. Comparison of β-scheme with $\beta = 1/3$ (left) and method 1, scheme 3 (right)

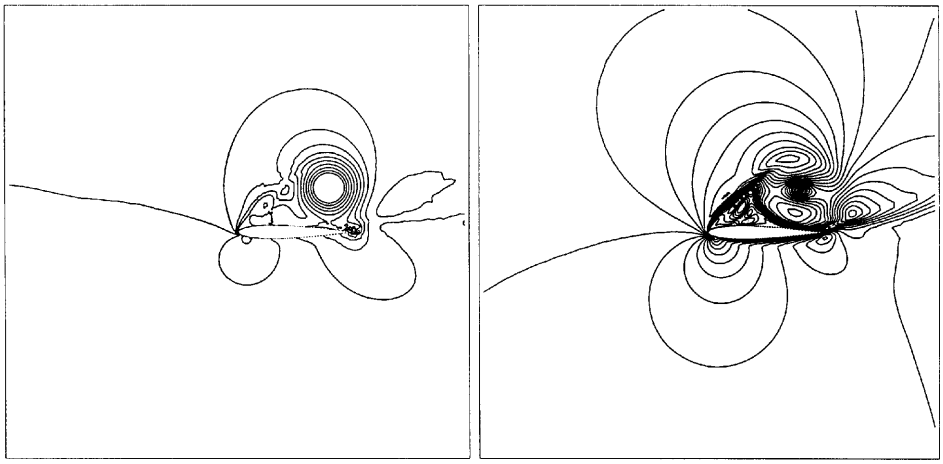

Figure 13. Method 1, scheme 3, fine mesh

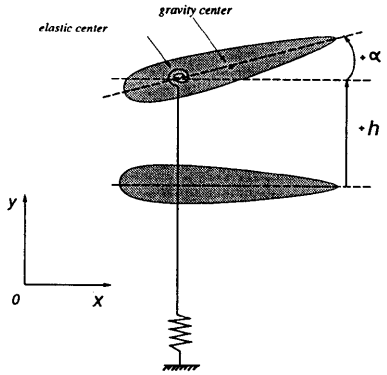

Figure 14. Description of aerofoil with two degrees of freedom

A weak coupling algorithm is used to solve the fluid–structure interaction system (14). The differential system of the structure is computed independently of the Euler equations. The following staggered procedure is used:

(i) $t = T^n$: W^n, q^n and $\dot{q}^n$
(ii) $Q^n(W) = Q(W^n)$
(iii) solving the equations of the structure
(iv) mesh moving
(v) solving the Euler equations.

We present aeroelastic results for the aerofoil using the different schemes.
As a preliminary we define the following data which characterize the structure:

(a) the non-dimensional distance from the elastic axis to the mass centre, $x_\alpha = S_\alpha/mb = 1{\cdot}8$, where m is the total mass of the structure, S_α denotes the static imbalance of the aerofoil about its elastic axis and b is the aerofoil semichord
(b) the inertial moment $v^2 = I_\alpha/mb^2 = 1{\cdot}865$, where I_α denotes the mass moment of inertia of the aerofoil about its elastic axis
(c) the frequency of bending, $\omega_h^2 = k_h/m = 100$ rad s^{-1}, and the frequency of torsion, $\omega_\alpha^2 = k_\alpha/I_\alpha = 100$ rad s^{-1}, where k_h and k_α respectively denote the total stiffness of the bending and the spring torsion.
(d) the absorption $\xi_h = C_h/2\omega_h m = 0$ and $\xi_\alpha = C_\alpha/2\omega_\alpha I_\alpha = 0$, where C_h and C_α respectively denote the absorption coefficients of translation and rotation
(e) the mass ratio $\mu = m/\pi\rho_\infty b^2 = 60$.

We consider a transonic flow (Mach number $M_\infty = 0{\cdot}8$ and zero angle of attack) which is initialized with the steady solution. The unstructured mesh used is composed of 800 nodes. At the initial time a small disturbance is imposed on the structure through the initial condition $(\mathrm{d}/\mathrm{d}t)\alpha(0) = -0{\cdot}01$. The object of the numerical study is to analyse the aeroelastic response of the structure according to the kind of flow; in particular, we want to observe the non-dimensional dynamic pressure at flutter, $\bar{Q} = (U_\infty/b\omega_\alpha\sqrt{\mu})^2$. Depending on the value of $\bar{Q}$, the aeroelastic response of the structure is stable, absorbed or amplified. We thus want to determine the value of $\bar{Q}$ which corresponds to null amplification.

Results are obtained with an implicit ($\Delta t = T/500$) upwind finite volume method with sixth-order dissipation terms (Section 3.1). Comparisons are made between the different versions of the new

scheme and the results of Rauch *et al.* obtained on a rather fine mesh with 2908 nodes[13] for the value of $\bar{Q} = 0{\cdot}5$. We present in Figure 15 the evolution of the rotation angle of the aerofoil and of two modes of the rotation. We observe that using method 1, scheme 3 and method 3, scheme 3 gives a neutrally stable aeroleastic response, whereas the β-scheme with $\beta = 1/3$ amplifies the rotation angle. The new schemes give a good representation of the evolution of the second mode (high-frequency mode), which is stable.

The amplification coefficient σ and the pulsation ω are evaluated and compared with those obtained by Rauch *et al.* (see Table II). These quantities are estimated through the modal components of the response assuming that the amplification coefficient follows an exponential rule ($f_i(t) = A \exp(\sigma t) \sin(\omega t)$. In comparison with the classical β-scheme, we firstly remark that the new scheme improves the determination of the value of the amplification coefficient, which must vanish for $\bar{Q} = 0{\cdot}5$. In comparison with the results obtained by Rauch *et al.* on a mesh with 2908 nodes, our new scheme is able to give a satisfactory prediction of the amplification and rotation coefficients even on a very coarse mesh.

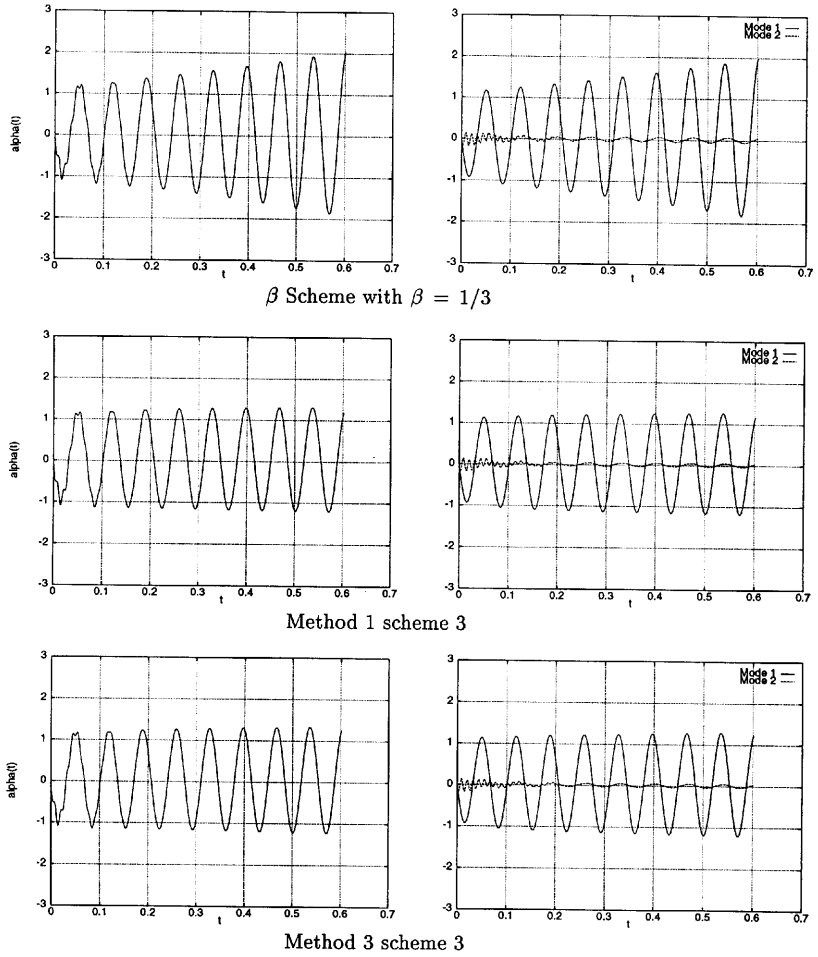

Figure 15. Evolution of rotation $\alpha(t)$ (deg) of aerofoil and of two modal components of $\alpha(t)$ for $\bar{Q} = 0{\cdot}5$ using different implicit ($\Delta t = T/500$) versions of new scheme on mesh with 800 nodes

Table II. Comparison of amplification and pulsation rates σ and ω respectively for $\bar{Q}=0{\cdot}5$ obtained with different versions of new scheme and explicit code of Rauch *et al.*[13]

		Mode 1		Mode 2	
Δt	Method	σ/ω_α	ω/ω_α	σ/ω_α	ω/ω_α
Explicit	Rauch *et al.*	0·000	0·913	0·148	5·349
Implicit	β-Scheme ($\beta=1/3$)	9·42E-03	9·09E-01	−5·37E-02	5·355
$T/500$	Method 1, scheme 3	4·12E-03	9·04E-01	−5·47E-02	5·342
	Method 3, scheme 3	4·09E-03	9·06E-01	−5·65E-02	5·346

5. FURTHER COMMENTS

This paper is dedicated to variational methods applicable to P1 variable representation. The first part evaluates the impact of fourth-order dissipations. The new scheme introduced in the second part carries a notable improvement in accuracy, particularly for unsteady flows; the stability is not much degraded (a courant number of 1·8 can be used) and the extra cost with respect to scheme 1 is 5%. Current investigations are being done with the aim of introducing a shock-capturing capability in this scheme.

REFERENCES

1. H. Paillère, H. Deconinck, R. Struijs, P. L. Roe, L. M. Mesaros and J. D. Muller, 'Computations of inviscid compressible flows using fluctuation-splitting on triangular meshes', *AIAA Paper 93-301*, 1993.
2. T. J. R. Hughes and M. Mallet, 'A new finite element formulation for computational fluid dynamics', *Comput. Methods Appl. Mech Eng.*, **58**, 329–336 (1986).
3. K. Mer, 'Variational analysis of a mixed finite element finite volume scheme on general triangulations', *INRIA Rep*, *2213*, 1994.
4. D. J. Mavriplis, A. Jameson and L. Martinelli, 'Multigrid solution of the Navier–Stokes equations on triangular meshes', *ICASE Rep. 89-11*, 1989.
5. P. Vankeirsbilck and H. Deconinck, 'Higher order upwind finite volume schemes with eno-properties for general unstructured meshes', *AGARD Rep. 787*, 1992.
6. K. Mer, 'Résultats sur la précision des schémas pour une loi de conservation linéaire', *INRIA Rep*., in preparation.
7. K. Mer, 'Variational Analysis of a Mixed Element/Volume Scheme with Fourth Order Viscosity on General Triangulations' INRIA Rep, 1996, and *Comput. Meth. Applied Mech. Engng*, in press, 1997.
8. A. Jameson, 'Artificial diffusion, upwind biasing, limiters and their effect on accuracy and multigrid convergence in transonic and hypersonic flows', *AIAA Paper* 93-3359, 1993.
9. J.-A. Desideri, A. Goudjo and V. Selmin, 'Third-order numerical schemes for hyperbolic problems', *INRIA Rep*., *607*, 1987.
10. R. Carpentier, 'Approximation d'écoulements instationnaires. Application à des instabilités tourbillonnaires', *Thesis*, Université de Nice-Sophia Antipolis, 1995.
11. H. Wu and L. Wang, 'Non-existence of third order accurate semidiscrete MUSCL-type schemes for nonlinear conservation laws and unified construction of high accurate ENO schemes', *Proc. Sixth Int. Symp. on Computational Fluid Dynamics*, Lake Tahoe, NV, September 1995.
12. K. Mer and B. Nkonga, 'Implicit calculations of an aeroelasticity problem', *Int. J. Comput. Fluid Dyn*., in press.
13. R. D. Rauch, J. T. Batina and H. T. Y. Yang, 'Euler flutter analysis of airfoils using unstructured dynamic meshes', *AIAA Paper 89-13837*, 1989.

